



**HAL**  
open science

# Kinetic characterization and molecular docking of novel allosteric inhibitors of aminoglycoside phosphotransferases

Nadia Leban, Elise Kaplan, Laurent Chaloin, Sylvain Godreuil, Corinne Lionne

## ► To cite this version:

Nadia Leban, Elise Kaplan, Laurent Chaloin, Sylvain Godreuil, Corinne Lionne. Kinetic characterization and molecular docking of novel allosteric inhibitors of aminoglycoside phosphotransferases. *Biochimica et Biophysica Acta (BBA) - General Subjects*, 2017, 1861 (1), pp.3464 - 3473. 10.1016/j.bbagen.2016.09.012 . hal-01809565

**HAL Id: hal-01809565**

**<https://hal.science/hal-01809565>**

Submitted on 30 Nov 2020

**HAL** is a multi-disciplinary open access archive for the deposit and dissemination of scientific research documents, whether they are published or not. The documents may come from teaching and research institutions in France or abroad, or from public or private research centers.

L'archive ouverte pluridisciplinaire **HAL**, est destinée au dépôt et à la diffusion de documents scientifiques de niveau recherche, publiés ou non, émanant des établissements d'enseignement et de recherche français ou étrangers, des laboratoires publics ou privés.

1           **Kinetic characterization and molecular docking of novel allosteric inhibitors of**  
2                           **aminoglycoside phosphotransferases**

3  
4       Nadia Leban <sup>a,1</sup>, Elise Kaplan <sup>a,2</sup>, Laurent Chaloin <sup>a</sup>, Sylvain Godreuil <sup>b</sup>, Corinne Lionne <sup>a,\*,3</sup>

5  
6       <sup>a</sup> CNRS FRE 3689 – Université de Montpellier, Centre d'études d'agents Pathogènes et  
7       Biotechnologies pour la Santé (CPBS), F-34293 Montpellier, France.

8       <sup>b</sup> INSERM U1058 – Université de Montpellier, Centre Hospitalier Régional Universitaire de  
9       Montpellier, Département de Bactériologie-Virologie, Montpellier, France.

10  
11       \* Corresponding author at: CBS, 29 rue de Navacelles, F-34090 Montpellier, France; Tel.:  
12       +33-(0)626-197-417; Fax : +33-(0)467-417-913.

13       E-mail address: corinne.lionne@cbs.cnrs.fr

14  
15       <sup>1</sup> Present address: Institut Supérieur de Biotechnologie de Monastir, Faculty of Pharmacy,  
16       University of Monastir, Tunisia.

17       <sup>2</sup> Present address: Department of Pathology, University of Cambridge, Cambridge, United  
18       Kingdom.

19       <sup>3</sup> Present address: Centre de Biochimie Structurale, CNRS UMR 5048 – Université de  
20       Montpellier – INSERM U 1054, Montpellier, France.

21  
22       *Abbreviations:* AME, aminoglycoside-modifying enzyme; AAC, aminoglycoside *N*-  
23       acetyltransferase; ANT, aminoglycoside *O*-nucleotidyltransferase; APH, aminoglycoside *O*-  
24       phosphotransferase; GOLD, Genetic Optimization for Ligand Docking.

25  
26       *Keywords:* allosteric inhibitors, antibiotic resistance, docking, inhibition modes, protein  
27       dynamics, steady state kinetics.

28 **ABSTRACT**

29

30 *Background:* Bacterial antibiotic resistance often leads to treatment failure which may have  
31 serious consequences, especially in critically sick patients. Resistance to aminoglycosides is  
32 mainly due to the expression of antibiotic-modifying enzymes. One important mechanism of  
33 aminoglycoside modification is the ATP/GTP-dependent O-phosphorylation catalyzed by  
34 aminoglycoside phosphotransferases, APHs. The aim of this study is to identify specific  
35 inhibitors of APHs that could restore bacterial susceptibility to aminoglycosides.

36 *Methods:* We focused on the search for allosteric inhibitors that bind to small cavities of the  
37 protein and block the enzyme function by perturbing its dynamics.

38 *Results:* From normal mode analysis, a cavity of variable volume belonging to a large groove  
39 which splits the protein into two parts was chosen as target. By molecular docking, we  
40 screened a large library of commercially available compounds. Seventeen of the highest  
41 ranked compounds were tested by *in vitro* kinetic experiments in order to evaluate their  
42 ability to inhibit APHs. Site-directed mutagenesis was carried out with the aim of confirming  
43 the inhibition mechanism determined kinetically and the interactions with the protein  
44 predicted by *in silico* studies. These interactions were also confirmed by the use of  
45 structurally-related molecules.

46 *Conclusions:* Two compounds showed interesting inhibition properties, and one was able to  
47 block two different classes of APH.

48 *General significance:* This study gives new insights into the inhibition of APHs by such  
49 allosteric inhibitors, and provides the basis for the future development of combined therapies,  
50 antibiotic plus APH inhibitor, which may reverse the resistance to aminoglycosides in a  
51 clinical context.

52

## 53 1. Introduction

54

55 Aminoglycosides constitute a large family of water soluble, polycationic amino sugars  
56 of considerable structural diversity. They are broad spectrum antibacterial agents that are  
57 products of bacterial or fungal metabolism. Bacterial resistance to aminoglycosides manifests  
58 itself by one of the following mechanisms: (i) the presence of aminoglycoside-modifying  
59 enzymes [1]; (ii) the decrease of bacteria membrane permeability towards aminoglycoside  
60 uptake into the bacteria or extrusion of the aminoglycosides from the cell by efflux pumps [2];  
61 or (iii) the modification of the drug target which can be either mutations that result in  
62 structural alterations of the ribosome [3] or methylations by 16S rRNA methyltransferases  
63 which interferes with the aminoglycoside binding [4]. Among these mechanisms, inactivation  
64 by aminoglycoside-modifying enzymes (AMEs) is the most important both in terms of level  
65 and frequency of resistance conferred to the bacteria [5]. There are three types of AMEs,  
66 each of which transfers a functional group onto the aminoglycoside structure thereby  
67 inactivating the antibiotic: aminoglycoside *O*-nucleotidyltransferases (ANTs) transfer a  
68 nucleoside monophosphate from a nucleoside triphosphate on a hydroxyl group of the  
69 antibiotic; aminoglycoside *N*-acetyltransferases (AACs) transfer an acetyl group from acetyl-  
70 CoA on an amine group; and aminoglycoside *O*-phosphotransferases (APHs) transfer the  $\gamma$ -  
71 phosphate of a nucleoside triphosphate on a hydroxyl group [6]. Each family of enzymes  
72 consists of different isoenzymes that differ in substrate specificity and selectivity. At least 50  
73 different genes for AMEs have been identified in bacteria [1,7]. A number of bacteria also  
74 harbor a bifunctional enzyme that catalyzes both acetylation and phosphorylation [8,9].

75 In bacterial resistant isolates that possess antibiotic-inactivating enzymes, drugs are  
76 enzymatically modified when they penetrate into the bacteria. Therefore, the altered drug is  
77 unable to interact efficiently with its target, the ribosome. Moreover, in the absence of active  
78 aminoglycosides that normally perturb bacterial protein synthesis, the next step of high-rate  
79 accumulation of antibiotic does not take place [10,11]. Since the discovery of the antibiotic-  
80 inactivating enzymes, many efforts have been carried out in order to chemically modify the

81 existing antibiotics and produce new drugs that retain their antibacterial activity without being  
82 inactivated. This strategy has led to considerable success, especially in the fight against  
83 penicillin resistance. For instance, the use of methicillin, a derivative of the early penicillins,  
84 overcame enzyme-mediated inactivation in most penicillin-resistant, gram-positive organisms  
85 [12]. Another strategy to overcome enzyme-associated resistance consists in combining the  
86 antibiotics with an inhibitor of the corresponding modifying enzyme. For example beta-  
87 lactamase inhibitors, such as clavulanic acid, associated with amoxicillin inhibit most strains  
88 of penicillinase-producing *S. aureus*, *H. influenza*, *E. coli*, *Klebsiella* spp,... [13]. Based on  
89 this strategy, several teams have searched for AMEs inhibitors. The new discovery of AAC  
90 inhibition by metal salts (mechanism still unknown) may offer a promising therapeutic issue  
91 [14,15]. Shi *et al.* reviewed recent progresses in development of APHs inhibitors [16]. The  
92 success in discovering specific inhibitors for AMEs depends on our ability to understand the  
93 basic properties of their mode of action and of their substrate specificity. So far, main studies  
94 focused on the development of competitive inhibitors that target either the nucleotide binding  
95 site, such as protein kinase inhibitors [17,18], or the aminoglycoside binding site, with  
96 aminoglycoside analogues [19,20] or non-carbohydrate inhibitors [21]. Using *in silico*  
97 screening of chemical libraries in the aminoglycoside binding site of AAC(6')-Ib, competitive  
98 inhibitors were recently identified [22].

99         However, therapeutic enzyme inhibitors are not restricted to active site competitors.  
100 Identification of small molecules that stabilize inactive conformations of the protein may  
101 represent a powerful starting point for rational drug design. The underlying idea is to complex  
102 the enzyme with a molecule that binds to a cavity other than the active site, and stabilizes the  
103 enzyme in a non-catalytically competent conformation. For example, the inhibition of  
104 APH(3')-IIIa by AR\_3a, an ankyrin repeat protein, has been shown to be due to a significant  
105 change of the APH conformation upon AR\_3a allosteric binding [23]. However, the large size  
106 of this modulator makes it hardly druggable.

107         Here, using normal mode analysis on two different APH crystal structures, we  
108 identified a common cavity of variable volume and used it as target for screening a library of

109 small commercially available compounds. By molecular docking, several potential allosteric  
110 inhibitors against two aminoglycoside-modifying enzymes, aminoglycoside 3'-  
111 phosphotransferase type IIIa, APH(3')-IIIa, and aminoglycoside 2"-phosphotransferase type  
112 IVa, APH(2")-IVa, were identified. We performed kinetic and molecular modelling studies to  
113 assess their mechanism of inhibition and to spotlight their binding site in the protein.  
114

## 115 **2. Materials and methods**

116

### 117 *2.1. Normal mode analysis and molecular docking*

118

119 Two starting crystal structures of APH(3')-IIIa (PDB ID: 1L8T, including kanamycin A  
120 and ADP, from [24]) and APH(2'')-IVa (PDB ID: 3SG8, including tobramycin, from [25]) were  
121 selected for normal modes computation and cavity search. In these structures, the  
122 aminoglycosides were removed to favour the binding of inhibitors near the target cavity. ADP  
123 was maintained in 1L8T, except otherwise stated in the text. The first two hundreds normal  
124 modes were calculated (all-atoms parameter set 27) using the VIBRAN module of CHARMM  
125 program [26,27] allowing to define fifty conformations for each enzyme. Briefly, after addition  
126 of hydrogen using the H-build routine, the potential energy of each system was minimized for  
127 5,000 steps of conjugate gradient algorithm (tolerance gradient of 0.01 kcal/mol/Å) followed  
128 by 50,000 steps of Adopted Basis Newton-Raphson to reach a mean energy gradient of less  
129 than  $10^{-5}$  kcal/mol/Å. Diagonalization of the Hessian matrix and normal modes were  
130 computed from these energy-minimized structures. Trajectories of superimposed modes  
131 (modes 7 to 200, after removal of the six first modes corresponding to intrinsic translational  
132 or rotational motions) were computed with CHARMM to produce fifty frames corresponding to  
133 protein conformers (hereafter called "trajectory" allowing to visualize the displacement of the  
134 whole coordinates on the superposed modes 7 to 200). Atomic fluctuations averaged by  
135 residues were computed from normal modes 7-200 using the fluctuation subroutine  
136 implemented in the Vibran module of Charmm. Structure and normal modes trajectories were  
137 analyzed with VMD software [28]. From these conformers, all cavities were identified and  
138 characterized using MDpocket software [29], and a small cavity fulfilling the criteria for  
139 allosteric inhibition (location and variable volume) located behind the kanamycin binding site  
140 was selected for subsequent screening.

141 All docking was performed using GOLD (Genetic Optimization for Ligand Docking)  
142 program v5.2 [30,31]. Zinc database (<http://zinc.docking.org>) [32] was queried to find drug-

143 like molecules according to Lipinski's rule-of-five [33]. Briefly, 100,000 compounds from the  
144 Zinc database were selected after applying these drug-like filtering criteria, except that logP  
145 was defined below or equal to 2 in order to increase the selection of aqueous-soluble  
146 compounds. All these molecules were screened by ensemble docking on both APHs using  
147 20 genetic algorithm runs within a 15 Å radius of the sphere centered on the targeted site  
148 and using Goldscore as scoring function. The docking poses were analyzed by the clustering  
149 method (complete linkage) from the rmsd matrix of ranking solutions. A second round of  
150 molecular docking (50 genetic algorithm runs) was performed on each APH separately, using  
151 the highest ranked compounds (the first hundred) from the ensemble screening. Twenty one  
152 compounds corresponding to the highest scores were selected, but finally, only seventeen  
153 compounds were commercially available and purchased.

154 Structural analysis and visualization of docking poses were carried out using the  
155 PyMOL Molecular Graphics System (version 1.3, Schrödinger, LLC).

156

## 157 2.2. Kinetic studies

158

159 In all *in vitro* kinetic experiments, equimolar concentrations of MgCl<sub>2</sub> were added to  
160 ATP. Thus, in the text, ATP and ADP refer to MgATP and MgADP, respectively.  
161 Experimental buffer was 50 mM Tris-HCl pH 7.5, 1 mM free MgCl<sub>2</sub>, 40 mM KCl, and the  
162 temperature was 25°C. The APH steady-state activity was evaluated using purified  
163 recombinant proteins, produced as previously reported [34], by measuring the time courses  
164 of ADP production by two different methods.

165 For a rapid screening of the compounds, the steady-state rate constants,  $k_{ss}$ , of  
166 enzyme activity were monitored in 96-well plates by coupling the release of ADP to a  
167 pyruvate kinase/lactate dehydrogenase reaction, as described by McKay *et al.* [35]. Reaction  
168 mixtures contained 0.5 μM APH, 4 mM phosphoenol pyruvate, 280 μM NADH, 20 U/ml  
169 pyruvate kinase, 25 U/ml lactate dehydrogenase, 25 or 350 μM ATP and 50 or 100 μM  
170 kanamycin A, with APH(3')-IIIa or APH(2'')-IVa, respectively. Experiments were carried out in



171 the absence or in the presence of potential inhibitors at 500  $\mu\text{M}$ . Reactions were initiated by  
172 the addition of ATP and monitored by reading the absorbance at 340 nm every 11 seconds.  
173 Values of  $k_{\text{ss}}$  were determined from the slope of linear phase of the reaction time courses  
174 using GraFit 7.0.2 software. The experiments were carried out in triplicate and the averaged  
175 inhibition was computed.

176 For the best compounds identified by the previously described enzymatic coupled  
177 system, the inhibition constants and inhibition modes were determined by the quench-flow  
178 method and HPLC analysis as previously described [36]. Briefly, quench-flow method  
179 consists in interrupting enzymatic reactions at different times with a quencher, which is  
180 usually a strong acid [37]. Here, 10% perchloric acid was used to stop the reaction every 3–  
181 7 s, depending on the enzyme. The reaction was triggered by addition of ATP in a  
182 thermostatically-controlled beaker (25°C) containing the enzyme and the aminoglycoside,  
183 with or without inhibitor. After quenching, the separation of ADP and ATP was carried out  
184 using HPLC (Alliance, Waters) and a partisphere SAX column (AIT France). The mobile  
185 phase was 200 mM ammonium phosphate buffer pH 5.5 and 10% acetonitrile. Samples from  
186 quench-flow were first spin at 19,000 g for 20 min at 4°C to remove precipitated protein. A  
187 volume of 100  $\mu\text{l}$  of supernatant quenched sample was diluted into 900  $\mu\text{l}$  of mobile phase  
188 supplemented with KOH to readjust the pH to 5.5. Volumes of 50 or 100  $\mu\text{l}$  of these samples  
189 were injected on the HPLC column. Quantification of ADP and ATP was obtained by  
190 integrating absorption peaks at 259 nm from the chromatograms. The inhibition mode and  
191 inhibition constants were determined by repeating the experiment at different concentrations  
192 of ATP (keeping kanamycin A concentration constant, see figure legends) or at different  
193 concentrations of kanamycin A (ATP concentration constant). APH concentrations were 0.1–  
194 0.5  $\mu\text{M}$ . Fittings were performed using GraFit 7.0.2 software using four different inhibition  
195 modes: competitive, non-competitive, uncompetitive and mixed. Only the most appropriate fit  
196 (which describes the inhibition with the lowest  $\text{Chi}^2$ ) is shown on the figures with the  
197 corresponding Lineweaver-Burk representation.

198

199 2.3. Site-directed mutagenesis

200

201 R211A mutant of APH(3')-IIIa was constructed by PCR (QuickChange Lightning Multi  
202 Site-Directed Mutagenesis Kit) using the two primers :

203 5'-TTTATTGATCTTGGGGCAAGCGGCAGGGCGGAC-3,' and

204 5'-GTCCGCCCTGCCGCTTGCCCCAAGATCAATAAA-3'.

205 Each 50 µl PCR reaction contained 2.5 µl of 10× QuickChange Lightning Multi  
206 reaction buffer, 0.75 µl of QuickSolution, 100 ng of DNA template (wild type *aph(3')-IIIa* in a  
207 pET15b plasmid), 1 µl of each mutagenic primer (100 ng), 10 mM dNTP and 2.5 units of  
208 QuickChange Lightning Multi enzyme blend. The PCR product was digested by DpnI  
209 restriction endonuclease for 1 h at 37°C. Mutant plasmids were recovered after  
210 transformation in *E. coli* BL21 (DE3) chemo-competent cells. Successful introduction of the  
211 desired mutations was controlled by sequencing the plasmid DNA (Fig. S1).

212 The mutant APH(3')-IIIa was produced in *E. coli* and purified as the wild type protein.

213

## 214 **3. Results**

215

### 216 *3.1. Target cavity identification by normal mode analysis*

217

218 Here, we focused on the search for APH allosteric inhibitors that bind to small cavities  
219 of the protein and block the enzyme function by perturbing its dynamics. Thus, a specific  
220 cavity was defined according to the following criteria: the cavity must be present in different  
221 APH subfamilies, it must be outside of the substrate binding sites, and lastly, it must undergo  
222 obvious volume change during the dynamics of the enzyme, required for its function. Sub-  
223 families APH(3') and APH(2'') were chosen because of their prevalence [1].

224 From the normal mode analysis, one cavity behind the aminoglycoside binding site  
225 was selected because it was fulfilling all the predefined criteria (Fig. 1, Fig. S2 also showing  
226 videos). It belongs to a large groove which splits the proteins into two parts. Moreover, the  
227 region defining this cavity was found to be flexible according to the fluctuations computed  
228 from the superposed normal modes (Fig. 1). It must be emphasized that the observed atomic  
229 fluctuations were relatively small and therefore were not considered as the main criteria to  
230 select the cavity (commonly, fluctuations of residues located at the interior of the protein are  
231 less important compared to external flexible loops). Typically, APH proteins do not require  
232 large collective motions like other kinases for their biological function and this feature renders  
233 more difficult the search for internal dynamic cavities. Nevertheless and taking into account  
234 to these small fluctuations, the target binding pocket was also selected in respect to the  
235 volume changes observed along the normal modes. The target cavities were surrounded by  
236 residues Gly192 and Arg226 in 1L8T structure and by residues Ser199 and Ser232 in 3SG8  
237 (yellow balls in Fig. S2). They are situated at a similar place within the two APHs and their  
238 compositions in amino acids were similar but not identical (at least one Phe, Leu, Ile, Ser and  
239 Asp found in each case).

240

### 240 **Figure 1**

241

### 242 3.2. Molecular docking

243

244 Using the targeted cavity defined above in APH(3')-IIIa and APH(2'')-IVa structures  
245 and the ZINC chemicals database [32], a virtual screening was carried out in order to predict  
246 and evaluate the potential affinity of these enzymes for drug-like molecules using Gold  
247 software. The Goldscore scoring function was used to rank the screened molecules – the  
248 highest scores predict highest affinities. In order to favor the binding of inhibitors near the  
249 target cavity which is located behind the aminoglycoside binding site, kanamycin A was  
250 removed from 1L8T structure (but not ADP) and tobramycin from 3SG8 prior docking.

251 In a first case study using an ensemble docking after overlaying both APH (same  
252 center of coordinates defining the target cavity at the same location for the two APHs), the  
253 first 100 out of the 100,000 compounds from the drug-like ZINC subset were selected based  
254 on their docking scores. Then, a second thorough docking run (50 GA runs) was performed  
255 on each APH separately with these selected compounds. We finally selected 21 best ranking  
256 ligands ( $63 < \text{score} < 81$ ) after named NL1 to NL21 (Table 1). NL4, NL7, NL10 and NL15  
257 were not commercially available, and therefore only 17 NL compounds were purchased for  
258 the further experimental assays.

259

### 260 3.3. Rapid *in vitro* screening of APH inhibitors using a coupled enzyme kinetic assay.

261

262 To evaluate the potential APH inhibition promoted by the selected molecules, *in vitro*  
263 inhibition studies were performed. The 17 molecules were rapidly screened using an  
264 enzymatic coupled-system, as previously described [35]. We used kanamycin A for these  
265 studies because both APHs can phosphorylate this aminoglycoside with a good efficiency  
266 through a Michaelis-Menten kinetics. Steady-state rate constants ( $k_{ss}$ ) were measured at  
267 fixed concentrations of ATP and kanamycin A, in the absence or in the presence of NL  
268 compounds (500  $\mu\text{M}$ ). Percentages of inhibition by NL compounds were determined and  
269 normalized in respect to the activity without compound. The results are summarized in Table

270 1. In these conditions, a 40% or higher inhibition of APH(3')-IIIa activity was observed with  
271 compounds NL6 and NL8, and for APH(2'')-IVa with compounds NL6, NL9 and NL16. Two  
272 compounds seemed particularly interesting: NL8 because it inhibits APH(3')-IIIa by almost  
273 80%, and NL6 for its ability to inhibit both APHs.

274 In order to determine the inhibition mode of these two compounds, steady-state  
275 kinetic experiments were carried out using a direct quenched-flow method. Results are  
276 described below and their mechanism is discussed on the basis of docking experiments.

277

### 278 3.3.1. Inhibition by NL8 compound.

279

280 NL8 was the most potent inhibitor amongst the 17 molecules tested here by the  
281 coupled system, showing a 79% inhibition of APH(3')-IIIa activity at 500  $\mu\text{M}$ . However, it  
282 showed little inhibition of APH(2'')-IVa activity. The steady-state rate constants,  $k_{\text{ss}}$ , of  
283 APH(3')-IIIa were determined at different concentrations of kanamycin A or ATP, and at 0, 50  
284 or 100  $\mu\text{M}$  concentrations of NL8 by the quenched-flow method. Double reciprocal plots of  
285  $1/k_{\text{ss}}$  versus  $1/[\text{ATP}]$  or  $1/[\text{kanamycin A}]$  are shown in Fig. 2.

286

### Figure 2

287 The NL8 compound was found to be a competitive inhibitor of APH(3')-IIIa towards  
288 ATP with a  $K_i$  of  $9 \pm 2 \mu\text{M}$ , and a non-competitive inhibitor towards kanamycin A with a  $K_i$  of  
289  $55 \pm 2 \mu\text{M}$ .

290 It should be noted that NL8 was initially identified as potential allosteric inhibitor on  
291 the basis of a docking on APH(3')-IIIa-ADP complex. To explain the unexpected ATP  
292 competitive inhibition mode found here, we carried out another docking of NL8 but in the  
293 absence of ADP (Fig. S3). In these conditions, NL8 was found to overlap with the nucleotide  
294 binding site, especially with the phosphate groups of the nucleotide. Unfortunately, it was  
295 difficult to predict with accuracy the binding of NL8 as the molecule presents a high degree of  
296 variability, even within repetitions of dockings (several rounds using identical parameters).

297 Similar variabilities were obtained when NL8 was docked in the apo, in the kanamycin-bound  
298 or in the ADP-bound structures.

299 NL8 was identified on the basis of an *in silico* screening in which the cavity of the  
300 targeted protein was located behind the aminoglycoside binding pocket (Fig. 1). However,  
301 the competition between ATP and NL8 upon binding to APH(3')-IIIa suggests that the  
302 inhibitor may bind to a different location, presumably closer to the nucleotide binding pocket  
303 without interfering with the aminoglycoside site.

304

### 305 3.3.2. Inhibition by NL6 compound.

306

307 The coupled enzyme system method showed that NL6 inhibited efficiently both  
308 enzymes with 43% and 63% inhibition for APH(3')-IIIa and APH(2'')-IVa, respectively.

309 We determined the mode of inhibition of each protein by NL6. Fig. 3A and B show  
310 that NL6 is a non-competitive inhibitor of APH(2'')-IVa towards both ATP and kanamycin A  
311 with  $K_i$  of  $85 \pm 10 \mu\text{M}$  and  $74 \pm 4 \mu\text{M}$ , respectively. Similarly, kinetics with APH(3')-IIIa showed  
312 NL6 acts again as a non-competitive inhibitor towards ATP and kanamycin A with  $K_i$  of  
313  $75 \pm 3 \mu\text{M}$  and  $76 \pm 6 \mu\text{M}$ , respectively (Fig. 3C and D).

314

### 314 **Figure 3**

315 To further investigate the binding of NL6 to APH(3')-IIIa, molecular docking of NL6  
316 was performed in the apo protein, in the ADP-bound structure and in the ternary complex  
317 (PDB ID: 1L8T). Although NL6 is acting on both APHs' activity, it was more difficult to predict  
318 the binding position of NL6 in APH(2'')-IVa. Therefore, we focused on APH(3')-IIIa here. A  
319 cluster of the best docking poses is shown in Fig. 4A, B, C for each simulation. Interestingly,  
320 if one part of the molecule presents an important degree of flexibility in the apo and in the  
321 ADP-bound structures, the dihydro-benzopyran ring of NL6 shows a rigorously identical  
322 location in all docking predictions, suggesting the importance of this group for NL6 binding.  
323 The interactions occurring between this moiety and the protein are detailed in Fig. 4D.

324

### 324 **Figure 4**

325 All molecular dockings predicted that the dihydro-benzopyran ring is stabilized by the  
326 backbone atoms of Leu209 and Gly210 and by a hydrogen bond between the carbonyl near  
327 the benzopyran ring and the side chain of Arg211 (Fig. 4D). This latter interaction seems to  
328 be of a crucial importance to stabilize the molecule as NL6 presents a completely different  
329 predicted location when Arg211 is replaced by an alanine (Fig. 4E). To assess the  
330 importance of this interaction for the *in vitro* binding of NL6, we engineered the R211A  
331 mutant of APH(3')-IIIa and performed kinetic studies in the absence or in the presence of  
332 NL6. The activity of this mutant was significantly affected:  $k_{cat}$  was decreased by 62%.  
333 Interestingly, the molecule was completely unable to inhibit the APH mutant (Fig. 4F). This  
334 result confirms the binding site of NL6 predicted by *in silico* studies and highlights the  
335 importance of Arg211 for its binding to APH.

336 To further investigate the importance of the two other interactions occurring with the  
337 benzopyran ring, we tested the activity of structurally related compounds. Indeed, the  
338 benzopyran moiety is stabilized by two hydrogen bonds with the backbones of Leu209 and  
339 Gly210, it was thus impossible to modify these interactions by mutations. Consequently, we  
340 evaluated the activity of two structurally related molecules. One of them, named NL6-1  
341 (Zinc14108604), contains the same dihydro-benzopyran ring than NL6 but with a slightly  
342 shorter structure, while the other compound, NL6-2 (Zinc13235262), has a naphthyl group  
343 instead. According to ZINC chemical database, the two analogues show more than 70% of  
344 structural similarity with NL6 (Fig. 5A).

345 Dockings were achieved in the APH(3')-IIIa with NL6 and its two analogues using the  
346 same parameters. According to these *in silico* studies, the two molecules bind to the same  
347 position to that observed for NL6 in the substrate-bound structure of APH(3')-IIIa (Fig. 5C and  
348 D). However, the naphthyl group of NL6-2 does not interact with the protein in contrast to the  
349 dihydro-benzopyran group NL6-1 which has similar interactions to those of NL6. Similarly,  
350 when docked in the apo protein, NL6 and NL6-1 show a strict overlay of their dihydro-  
351 benzopyran group, while NL6-2 presents a completely different binding mode (Fig. 5E and  
352 F). The naphthyl group of NL6-2 is indeed located at the opposite side from ADP in contrast

353 to the dihydro-benzopyran moiety of NL6 and NL6-1, located near the nucleotide binding site.  
354 This suggests that the benzopyran ring is also important for the stabilization of NL6.

355 **Figure 5**

356 Based on this prediction, these molecules were tested *in vitro* to estimate their ability  
357 to inhibit the APH(3')-IIIa activity. As shown in Fig. 5B, NL6-1 inhibits the activity of the APH.  
358 Similarly to NL6, NL6-1 was confirmed to act as a non-competitive inhibitor towards ATP with  
359 a  $K_i$  of  $185 \pm 12 \mu\text{M}$  (data not shown). The 2-fold higher  $K_i$  of NL6-1 compared to NL6 can be  
360 explained by its shorter structure (20 carbons) compared to NL6 (23 carbons), resulting in a  
361 smaller number of interactions with the protein and consequently in a weaker inhibition. In  
362 contrast, NL6-2 was completely unable to inhibit the APH activity, confirming the hypothesis  
363 that the dihydro-benzopyran group is of major importance for APH inhibition.

364 According to kinetic and molecular docking studies, NL6 is likely to bind between both  
365 substrates, without affecting their binding. The presence of NL6 should greatly perturb the  
366 phosphotransfer of the  $\gamma$ -phosphate of ATP on the 3'-OH of kanamycin A which could explain  
367 the enzyme inhibition.

368 To conclude, the dihydro-benzopyran ring is of crucial importance for the binding of  
369 NL6 to APH enzymes. In addition, the two interactions with side chain of Arg211 and  
370 backbones of Leu209 and Gly210 were shown to play an essential role in the inhibition of  
371 APH.

372  
373



#### 374 4. Discussion

375

376 The problem of bacterial resistance to antibiotic due to aminoglycoside  
377 phosphotransferases APH(2'')-IVa and APH(3')-IIIa enzymes could be overcome by the  
378 development of novel drugs that target APHs, as suggested by Shi and co-authors in a  
379 recent review [16]. For example, because of the structural similarity of the ATP binding  
380 domain with protein kinases, APHs can be inhibited by eukaryotic protein kinase inhibitors. In  
381 this way, protein kinase inhibitors of the isoquinoline sulfonamide family have been shown to  
382 be competitive inhibitors of APH(3')-IIIa towards ATP, although they were unable to restore  
383 aminoglycoside susceptibility of strains harboring *aph(3')-IIIa* gene [38]. In the same manner,  
384 Shakya *et al.* screened a library of known kinase inhibitors and identified pyrido-pyrimidines  
385 as selective inhibitors of APH(3')s and flavonoids as general inhibitors of APHs [39]. A crystal  
386 structure of the APH(2'')-IVa-kanamycin-quercetin complex allowed to confirm that the  
387 inhibitor binds to the ATP binding site of the enzyme.

388 The problem with such kinase inhibitors is their intrinsic poor selectivity because they  
389 target the ATP binding site of APHs which is similar to that of many eukaryotic important  
390 enzymes. However, the recent structure-guided optimization of protein kinase inhibitors  
391 constitutes a promising strategy to enhance their specificity for APHs [18]. The originality of  
392 our inhibitors, compared to these protein kinase inhibitors, is that they do not target the  
393 substrate binding site, hence avoiding or reducing off-target effects. Therefore, they are  
394 neither going to compete with the antibiotic itself for the binding to APHs or to the rRNA  
395 target, nor with ATP which has a central role in many physiological processes. Instead, they  
396 have been selected for their ability to interfere with important dynamic properties of the  
397 targeted enzyme.

398 A similar strategy was successfully applied to APH with the development of allosteric  
399 inhibitors based on engineered ankyrin repeat motives. These compounds inhibited the  
400 enzyme activity, both *in vitro* and *in vivo*, and were able to restore the bacteria sensitivity to  
401 kanamycin and amikacin to a level comparable to that of the corresponding knockout strains

402 [40]. Later, the resolution of the crystal structure of APH(3')-IIIa complexed with one of the  
403 most potent ankyrin repeat protein inhibitor has confirmed the allosteric inhibition mechanism  
404 [23]. Indeed, the binding of the inhibitor stabilizes the APH in a non-catalytically competent  
405 conformation. However, the designed ankyrin repeat protein is a large molecule that is hardly  
406 druggable.

407 Here, on the basis of *in silico* screening of a chemical library, our idea was to find  
408 small molecules that are more druggable than large proteins and that inhibit APHs in a  
409 similar manner to that of ankyrin repeat protein. Allosteric small-molecule kinase inhibitors  
410 are indeed promising alternatives to active site binders, as recently reviewed [41].

411 We have identified twenty one small molecules that are potential allosteric inhibitors  
412 of APHs. Out of the seventeen that were evaluated, four molecules were able to inhibit  
413 significantly APH activity *in vitro*. We determined the mode of inhibition for two of them and  
414 showed that they are non-competitive towards kanamycin A. One of them, NL8, was a  
415 competitive inhibitor of APH(3')-IIIa towards ATP, suggesting that it should bind near the  
416 nucleotide binding position, but its precise binding position remains elusive. The fact that it  
417 did not inhibit APH(2'')-IVa suggests that it does not bind to the nucleotide binding site which  
418 is conserved between the two APHs. The most promising molecule, NL6, is able to inhibit  
419 non-competitively the two APHs tested. Its binding site was confirmed both by mutating one  
420 interacting residue of APH and by the use of NL6 analogues with one missing the dihydro-  
421 benzopyran ring required for an efficient binding. As shown in Fig. 6, NL6 binds to a different  
422 location in APH(3')-IIIa that of the protein kinase inhibitor CKI, and of the ankyrin-repeat  
423 protein inhibitor AR-3A.

### 424 **Figure 6**

425 This confirms that non-allosterically modulated proteins such as APHs can be  
426 inhibited by small druggable allosteric compounds, which brings new insights for the rational  
427 drug discovery of APHs inhibitors.

428 The seventeen compounds will be further tested for their effect on antibiotic  
429 susceptibility of different Gram-positive and Gram-negative bacteria strains as well as on

430 their potential cell toxicity. The integration of dynamic motions by using normal mode  
431 analysis in combination with molecular docking, enzyme kinetics and antibacterial activity  
432 studies, provided important insights into the molecular basis underlying ligand binding and  
433 enzyme inhibition. Co-crystallization assays of APHs with these molecules are currently in  
434 progress and rational lead optimization processes are considered in order to design new  
435 derivatives with higher inhibitory properties. Efforts should be made to increase the affinity of  
436 APH for the inhibitor by adding chemical substitutions that would interact with additional  
437 residues of the cavity. This should avoid that a single mutation of the protein is enough to  
438 prevent the inhibition.  
439

440 **5. Conclusion**

441

442 Optimization of the lead compounds identified in this study should help in the design  
443 of efficient APHs inhibitors that may overcome APH-dependent bacterial resistance to  
444 aminoglycosides. Emergence and frequency of potential resistance mutants will be evaluated  
445 *in vitro*. Moreover, this strategy may be applied to other multi-resistant strains for which the  
446 major AMEs have been identified.

447

448

449 **Acknowledgment**

450

451           This work was supported by the Centre National de la Recherche Scientifique  
452 (CNRS), the University of Montpellier and the Agence Nationale de la Recherche (ANR  
453 Programme Blanc 2011-SIMI7, "cN-II Focus"). France-Tunisia exchange was supported by a  
454 CNRS program (EDC25987). Dr. Nadia Leban is grateful to the Infectiopôle Sud Foundation  
455 for a post-doctoral fellowship and Dr. Elise Kaplan to the Fondation pour la Recherche  
456 Médicale for doctoral fellowship (FDT20140931113).

457           We thank Professor Sergei B. Vakulenko (Notre Dame, USA) and Professor Engin H.  
458 Serpersu (Knoxville, USA) for the generous gift of the *aph(2'')-IVa* and *aph(3')-IIIa* genes. We  
459 thank Ms Perrine Lallemand (CPBS) for her help in the APH purification procedure.

460

461

462 **References**

463

464 [1] Ramirez MS & Tolmasky ME (2010) Aminoglycoside modifying enzymes. *Drug Resist.*  
465 *Updat.* **13**, 151–171.

466 [2] Kumar A & Schweizer HP (2005) Bacterial resistance to antibiotics: active efflux and  
467 reduced uptake. *Adv. Drug Deliv. Rev.* **57**, 1486–1513.

468 [3] Pfister P, Hobbie S, Vicens Q, Böttger EC & Westhof E (2003) The molecular basis for  
469 A-site mutations conferring aminoglycoside resistance: relationship between ribosomal  
470 susceptibility and X-ray crystal structures. *Chembiochem* **4**, 1078–1088.

471 [4] Doi Y & Arakawa Y (2007) 16S ribosomal RNA methylation: emerging resistance  
472 mechanism against aminoglycosides. *Clin. Infect. Dis.* **45**, 88–94.

473 [5] Vakulenko SB & Mobashery S (2003) Versatility of aminoglycosides and prospects for  
474 their future. *Clin. Microbiol. Rev.* **16**, 430–450.

475 [6] Wright GD, Berghuis AM & Mobashery S (1998) Aminoglycoside antibiotics. Structures,  
476 functions, and resistance. *Adv. Exp. Med. Biol.* **456**, 27–69.

477 [7] Shaw KJ, Rather PN, Hare RS & Miller GH (1993) Molecular genetics of  
478 aminoglycoside resistance genes and familial relationships of the aminoglycoside-  
479 modifying enzymes. *Microbiol. Rev.* **57**, 138–163.

480 [8] Ferretti JJ, Gilmore KS & Courvalin P (1986) Nucleotide sequence analysis of the gene  
481 specifying the bifunctional 6'-aminoglycoside acetyltransferase 2"-aminoglycoside  
482 phosphotransferase enzyme in *Streptococcus faecalis* and identification and cloning of  
483 gene regions specifying the two activities. *J. Bacteriol.* **167**, 631–638.

484 [9] Azucena E, Grapsas I & Mobashery S (1997) Properties of a bifunctional bacterial  
485 antibiotic resistance enzyme that catalyzes ATP-dependent 2"-phosphorylation and  
486 acetyl-CoA-dependent 6'-acetylation of aminoglycosides. *J. Am. Chem. Soc.* **119**,  
487 2317–2318.

488 [10] Dickie P, Bryan LE & Pickard MA (1978) Effect of enzymatic adenylation on  
489 dihydrostreptomycin accumulation in *Escherichia coli* carrying an R-factor: model

- 490 explaining aminoglycoside resistance by inactivating mechanisms. *Antimicrob. Agents*  
491 *Chemother.* **14**, 569–580.
- 492 [11] Höltje JV (1979) Induction of streptomycin uptake in resistant strains of *Escherichia*  
493 *coli*. *Antimicrob. Agents Chemother.* **15**, 177–181.
- 494 [12] Bush K & Mobashery S (1998) How beta-lactamases have driven pharmaceutical drug  
495 discovery. From mechanistic knowledge to clinical circumvention. *Adv. Exp. Med. Biol.*  
496 **456**, 71–98.
- 497 [13] Drawz SM & Bonomo RA (2010) Three decades of beta-lactamase inhibitors. *Clin.*  
498 *Microbiol. Rev.* **23**, 160–201.
- 499 [14] Chiem K, Fuentes BA, Lin DL, Tran T, Jackson A, Ramirez MS & Tolmasky ME (2015)  
500 Inhibition of aminoglycoside 6'-N-acetyltransferase type Ib-mediated amikacin  
501 resistance in *Klebsiella pneumoniae* by zinc and copper pyrithione. *Antimicrob. Agents*  
502 *Chemother.* **59**, 5851–5853.
- 503 [15] Li Y, Green KD, Johnson BR & Garneau-Tsodikova S (2015) Inhibition of  
504 aminoglycoside acetyltransferase resistance enzymes by metal salts. *Antimicrob.*  
505 *Agents Chemother.* **59**, 4148–4156.
- 506 [16] Shi K, Caldwell SJ, Fong DH & Berghuis AM (2013) Prospects for circumventing  
507 aminoglycoside kinase mediated antibiotic resistance. *Front. Cell. Infect. Microbiol.* **3**,  
508 22.
- 509 [17] Fong DH, Xiong B, Hwang J & Berghuis AM (2011) Crystal structures of two  
510 aminoglycoside kinases bound with a eukaryotic protein kinase inhibitor. *PLoS One* **6**,  
511 e19589.
- 512 [18] Stogios PJ, Spanogiannopoulos P, Evdokimova E, Egorova O, Shakya T, Todorovic N,  
513 Capretta A, Wright GD & Savchenko A (2013) Structure-guided optimization of protein  
514 kinase inhibitors reverses aminoglycoside antibiotic resistance. *Biochem. J.* **454**, 191–  
515 200.

- 516 [19] Szychowski J, Kondo J, Zahr O, Auclair K, Westhof E, Hanessian S & Keillor JW  
517 (2011) Inhibition of aminoglycoside-deactivating enzymes APH(3')-IIIa and AAC(6')-II  
518 by amphiphilic paromomycin O<sup>2</sup>-ether analogues. *ChemMedChem* **6**, 1961–1966.
- 519 [20] Vong K, Tam IS, Yan X & Auclair K (2012) Inhibitors of aminoglycoside resistance  
520 activated in cells. *ACS Chem. Biol.* **7**, 470–475.
- 521 [21] Welch KT, Virga KG, Whittemore NA, Özen C, Wright E, Brown CL, Lee RE &  
522 Serpersu EH (2005) Discovery of non-carbohydrate inhibitors of aminoglycoside-  
523 modifying enzymes. *Bioorg. Med. Chem.* **13**, 6252–6263.
- 524 [22] Lin DL, Tran T, Adams C, Alam JY, Herron SR & Tolmasky ME (2013) Inhibitors of the  
525 aminoglycoside 6'-N-acetyltransferase type Ib [AAC(6')-Ib] identified by *in silico*  
526 molecular docking. *Bioorg. Med. Chem. Lett.* **23**, 5694–5698.
- 527 [23] Kohl A, Amstutz P, Parizek P, Binz HK, Briand C, Capitani G, Forrer P, Plückthun A &  
528 Grütter MG (2005) Allosteric inhibition of aminoglycoside phosphotransferase by a  
529 designed ankyrin repeat protein. *Structure* **13**, 1131–1141.
- 530 [24] Fong DH & Berghuis AM (2002) Substrate promiscuity of an aminoglycoside antibiotic  
531 resistance enzyme via target mimicry. *EMBO J.* **21**, 2323–2331.
- 532 [25] Shi K, Houston DR & Berghuis AM (2011) Crystal structures of antibiotic-bound  
533 complexes of aminoglycoside 2"-phosphotransferase IVa highlight the diversity in  
534 substrate binding modes among aminoglycoside kinases. *Biochemistry* **50**, 6237–6244.
- 535 [26] Brooks BR, Brooks CL, Mackerell AD, Nilsson L, Petrella RJ, Roux B, Won Y,  
536 Archontis G, Bartels C, Boresch S, Caflisch A, Caves L, Cui Q, Dinner AR, Feig M,  
537 Fischer S, Gao J, Hodoscek M, Im W, Kuczera K, Lazaridis T, Ma J, Ovchinnikov V,  
538 Paci E, Pastor RW, Post CB, Pu JZ, Schaefer M, Tidor B, Venable RM, Woodcock HL,  
539 Wu X, Yang W, York DM & Karplus M (2009) CHARMM: the biomolecular simulation  
540 program. *J. Comput. Chem.* **30**, 1545–1614.
- 541 [27] Zhu X, Lopes PEM & Mackerell AD (2012) Recent Developments and Applications of  
542 the CHARMM force fields. *Wiley Interdiscip. Rev. Comput. Mol. Sci.* **2**, 167–185.



- 543 [28] Humphrey W, Dalke A & Schulten K (1996) VMD: visual molecular dynamics. *J. Mol.*  
544 *Graph.* **14**, 33–38, 27–28.
- 545 [29] Schmidtke P, Bidon-Chanal A, Luque FJ & Barril X (2011) MDpocket: open-source  
546 cavity detection and characterization on molecular dynamics trajectories.  
547 *Bioinformatics* **27**, 3276–3285.
- 548 [30] Jones G, Willett P & Glen RC (1995) Molecular recognition of receptor sites using a  
549 genetic algorithm with a description of desolvation. *J. Mol. Biol.* **245**, 43–53.
- 550 [31] Jones G, Willett P, Glen RC, Leach AR & Taylor R (1997) Development and validation  
551 of a genetic algorithm for flexible docking. *J. Mol. Biol.* **267**, 727–748.
- 552 [32] Irwin JJ, Sterling T, Mysinger MM, Bolstad ES & Coleman RG (2012) ZINC: a free tool  
553 to discover chemistry for biology. *J. Chem. Inf. Model.* **52**, 1757–1768.
- 554 [33] Lipinski CA (2004) Lead- and drug-like compounds: the rule-of-five revolution. *Drug*  
555 *Discov. Today Technol.* **1**, 337–341.
- 556 [34] Lallemand P, Leban N, Kunzelmann S, Chaloin L, Serpersu EH, Webb MR, Barman T  
557 & Lionne C (2012) Transient kinetics of aminoglycoside phosphotransferase(3')-IIIa  
558 reveals a potential drug target in the antibiotic resistance mechanism. *FEBS Lett.* **586**,  
559 4223–4227.
- 560 [35] McKay GA, Thompson PR & Wright GD (1994) Broad spectrum aminoglycoside  
561 phosphotransferase type III from *Enterococcus*: overexpression, purification, and  
562 substrate specificity. *Biochemistry* **33**, 6936–6944.
- 563 [36] Kaplan E, Guichou J-F, Chaloin L, Kunzelmann S, Leban N, Serpersu EH & Lionne C  
564 (2016) Aminoglycoside binding and catalysis specificity of aminoglycoside 2"-  
565 phosphotransferase IVa: A thermodynamic, structural and kinetic study. *Biochim.*  
566 *Biophys. Acta* **1860**, 802–813.
- 567 [37] Barman TE, Bellamy SRW, Gutfreund H, Halford SE & Lionne C (2006) The  
568 identification of chemical intermediates in enzyme catalysis by the rapid quench-flow  
569 technique. *Cell. Mol. Life Sci.* **63**, 2571–2583.

- 570 [38] Daigle DM, McKay GA & Wright GD (1997) Inhibition of aminoglycoside antibiotic  
571 resistance enzymes by protein kinase inhibitors. *J. Biol. Chem.* **272**, 24755–24758.
- 572 [39] Shakya T, Stogios PJ, Waglechner N, Evdokimova E, Ejim L, Blanchard JE, McArthur  
573 AG, Savchenko A & Wright GD (2011) A small molecule discrimination map of the  
574 antibiotic resistance kinome. *Chem. Biol.* **18**, 1591–1601.
- 575 [40] Amstutz P, Binz HK, Parizek P, Stumpp MT, Kohl A, Grütter MG, Forrer P & Plückthun  
576 A (2005) Intracellular kinase inhibitors selected from combinatorial libraries of designed  
577 ankyrin repeat proteins. *J. Biol. Chem.* **280**, 24715–24722.
- 578 [41] Wu P, Clausen MH & Nielsen TE (2015) Allosteric small-molecule kinase inhibitors.  
579 *Pharmacol. Ther.* **156**, 59–68.
- 580

581 **Figure captions**

582

583 **Fig. 1.** Identification of the target cavities using normal mode analysis. (A) Crystal structure of  
584 APH(3')-IIIa shown as blue cartoon, complexed with ADP and kanamycin A in stick  
585 representation (PDB ID: 1L8T). (B) Detection of all the dynamic cavities, shown in mesh  
586 representation, from the fifty frames of the trajectory of the 200 first normal modes of 1L8T  
587 structure depleted of ligands. (C) Selected cavity used for virtual screening. (D) Crystal  
588 structure of APH(2'')-IVa shown as pink cartoon, complexed with tobramycin in stick  
589 representation (PDB ID: 3SG8). (E) Detection of dynamic cavities of 3SG8 structure without  
590 tobramycin. (F) Selected cavity used for virtual screening. (G) Volume of the target cavities  
591 (shown in C and F) showing variation along the normal modes trajectory of APH(3')-IIIa (in  
592 blue) and APH(2'')-IVa (in red). (H and I) Atomic fluctuations averaged by residue computed  
593 from normal mode analysis for APH(3')-IIIa (1L8T) and APH(2'')-IVa, respectively. The  
594 numbers highlight residues showing significant fluctuations (for more details, see Fig. S2).

595

596 **Fig. 2.** Determination of APH(3')-IIIa inhibition mode by NL8. (A) Competitive inhibition profile  
597 by NL8 towards ATP. Final concentrations were 0.1  $\mu\text{M}$  APH(3')-IIIa, 50  $\mu\text{M}$  kanamycin A  
598 and 5–500  $\mu\text{M}$  ATP. (B) Non-competitive inhibition profile by NL8 towards kanamycin A. Final  
599 concentrations were 0.1  $\mu\text{M}$  APH(3')-IIIa, 5–200  $\mu\text{M}$  kanamycin A and 25  $\mu\text{M}$  ATP.  
600 Lineweaver-Burk representations are shown but the fits were carried out on raw data. NL8  
601 concentrations were 0  $\mu\text{M}$  (circles), 50  $\mu\text{M}$  (squares) or 100  $\mu\text{M}$  (triangles).

602

603 **Fig. 3.** Determination of the inhibition mode of APH(2'')-IVa (A, B) or APH(3')-IIIa (C, D) by  
604 NL6. Final concentrations were (A) 0.5  $\mu\text{M}$  APH(2'')-IVa, 100  $\mu\text{M}$  kanamycin A and 50–500  
605  $\mu\text{M}$  ATP; (B) 0.5  $\mu\text{M}$  APH(2'')-IVa, 5–150  $\mu\text{M}$  kanamycin A and 400  $\mu\text{M}$  ATP; (C) 0.1  $\mu\text{M}$   
606 APH(3')-IIIa, 50  $\mu\text{M}$  kanamycin A and 5–250  $\mu\text{M}$  ATP; (D) 0.1  $\mu\text{M}$  APH(3')-IIIa, 5–100  $\mu\text{M}$   
607 kanamycin A and 25  $\mu\text{M}$  ATP. NL6 concentrations were 0  $\mu\text{M}$  (circles), 20  $\mu\text{M}$  (triangles) or  
608 50  $\mu\text{M}$  (squares).

609

610 **Fig. 4.** (A, B, C) Clusters of docking poses of NL6 in the apo, in the ADP-bound and in the  
611 ternary structures of APH(3')-IIIa, respectively. The stable dihydro-benzopyran group of NL6  
612 is shown surrounded by a dashed line. (D) Details of interactions of the dihydro-benzopyran  
613 ring of NL6 with APH(3')-IIIa. (E) Docking of NL6 in the substrate-bound structure of APH(3')-  
614 IIIa R211A mutant. (F) Steady state activity of APH(3')-IIIa R211A mutant as a function of  
615 ATP concentration in the absence (circles) or in the presence of NL6 (squares). Final  
616 concentrations were 0.2  $\mu\text{M}$  R211A APH(3')-IIIa, 50  $\mu\text{M}$  kanamycin A, 5-100  $\mu\text{M}$  ATP, and 0  
617 or 50  $\mu\text{M}$  NL6.

618

619 **Fig. 5.** (A) Structure of NL6 and the two selected analogues, NL6-1 and NL6-2. (B)  
620 Comparison of APH(3')-IIIa steady state activity as a function of ATP concentration in the  
621 absence of NL compound (circles) or in the presence of NL6 (squares), NL6-1 (triangles) or  
622 NL6-2 (stars). Final concentrations were 0.1  $\mu\text{M}$  APH(3')-IIIa, 50  $\mu\text{M}$  kanamycin A, 5–100  $\mu\text{M}$   
623 ATP, and 0 or 50  $\mu\text{M}$  NL compounds. (C, D) Overlay of the best docking poses of NL6 (grey)  
624 and NL6-1 (pink) or NL6-2 (dark cyan) respectively in the APH(3')-IIIa-ADP·kanamycin A  
625 complex. (E, F) Overlay of the best docking poses of NL6 and NL6-1 or NL6-2 respectively in  
626 the apo structure of APH(3')-IIIa.

627

628 **Fig. 6.** (A, B) Crystal structures of the APH(3')-IIIa bound to CKI-inhibitor (yellow sticks, PDB  
629 ID: 3Q2J) or to AR\_3A inhibitor (green cartoon, PDB ID: 2BKK), respectively. (C) Predicted  
630 binding position of NL6 (grey sticks) in APH(3')-IIIa.

631

**Table 1.**

Docking scores and averaged *in vitro* APH inhibitions of selected NL compounds. Compounds that were not commercially available are indicated by an asterisk. Zinc numbers are indicated in brackets. Inhibitions of APH activity by 500  $\mu$ M of NL compound are expressed as percentage relative to the activity without compound. Inhibitions by 40% or more are highlighted in bold.

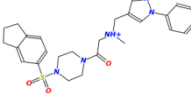
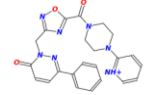
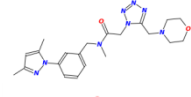
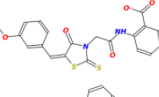
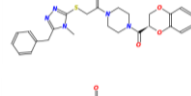
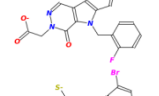
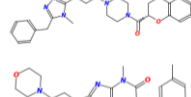
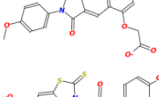
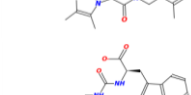
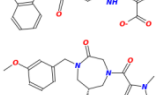
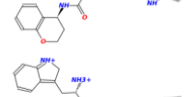
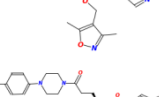
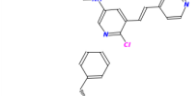
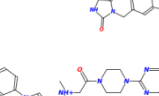
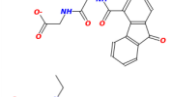
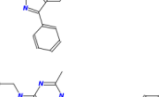
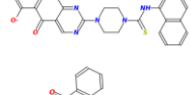
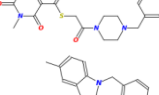
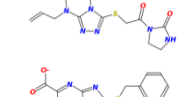
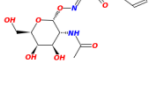
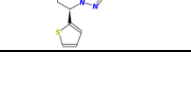
Compound (ZINC number)	Structure	APH(3')-IIIa		APH(2'')-IVa		Compound (ZINC number)	Structure	APH(3')-IIIa		APH(2'')-IVa	
		Score	Inhibition	Score	Inhibition			Score	Inhibition	Score	Inhibition
NL1 (08981682)		71	7	81	10	NL12 (40455179)		75	0	66	17
NL2 (20785546)		73	0	80	26	NL13 (1792615)		75	8	69	27
NL3 (13001091)		77	7	79	9	NL14 (6751595)		61	0	68	0
NL4* (13001089)		78	nd	78	nd	NL15* (36046879)		76	nd	69	nd
NL5 (22406103)		80	20	77	19	NL16 (13572054)		81	37	63	<b>68</b>
NL6 (13236811)		83	<b>43</b>	77	<b>63</b>	NL17 (14746000)		80	0	63	12
NL7* (52627502)		80	nd	77	nd	NL18 (36589946)		79	0	60	12
NL8 (8790387)		81	<b>79</b>	74	7	NL19 (8981627)		75	3	63	0
NL9 (1143187)		80	12	71	<b>45</b>	NL20 (22357542)		73	0	71	14
NL10* (05277506)		71	nd	68	nd	NL21 (12636347)		64	37	63	24
NL11 (20737652)		67	2	64	14						

Figure 1

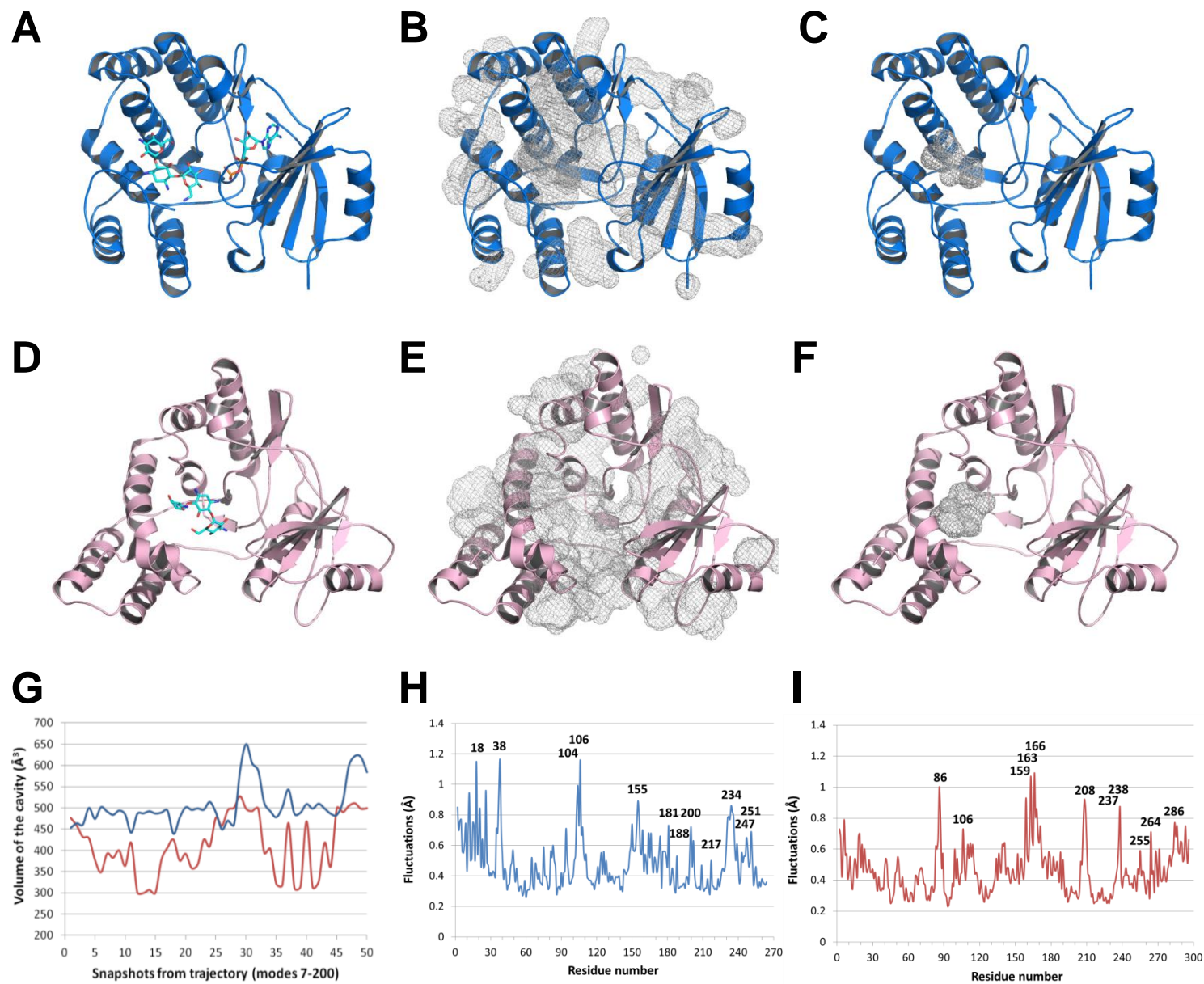


Figure 2

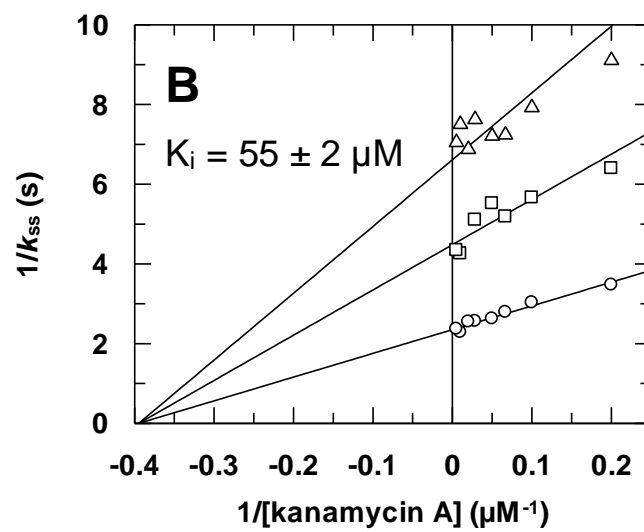
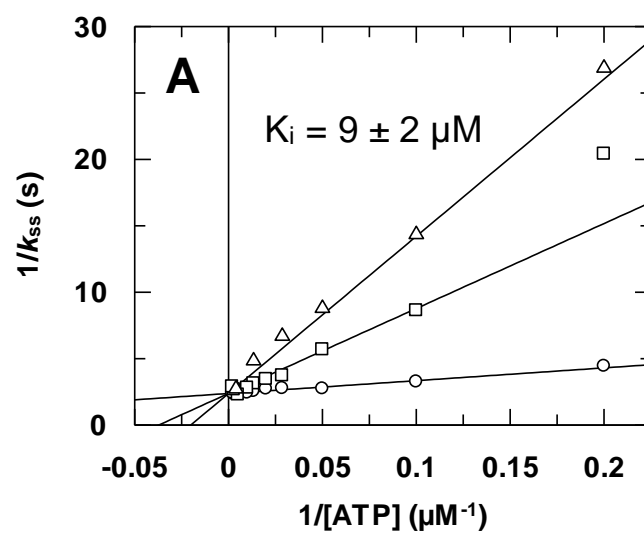


Figure 3

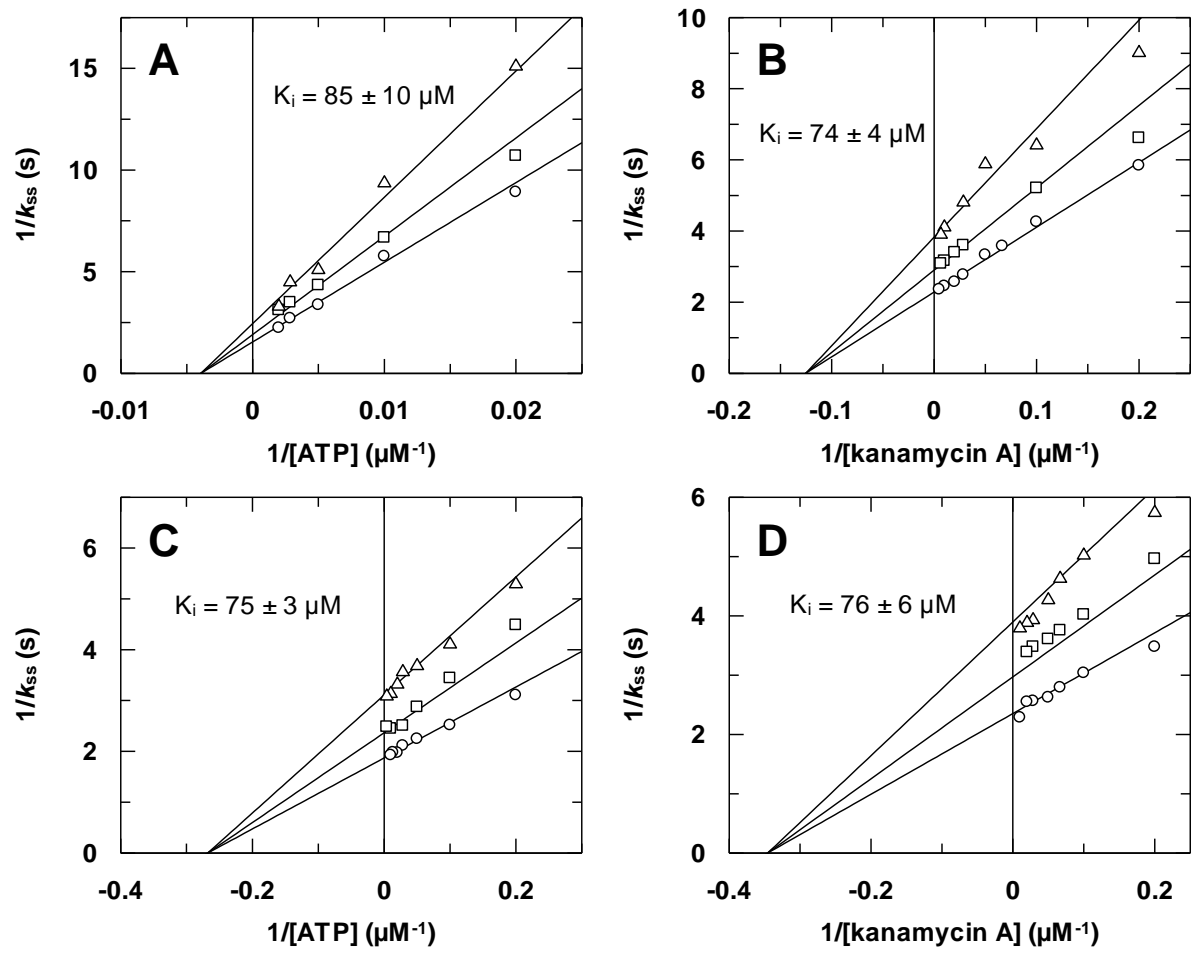




Figure 4

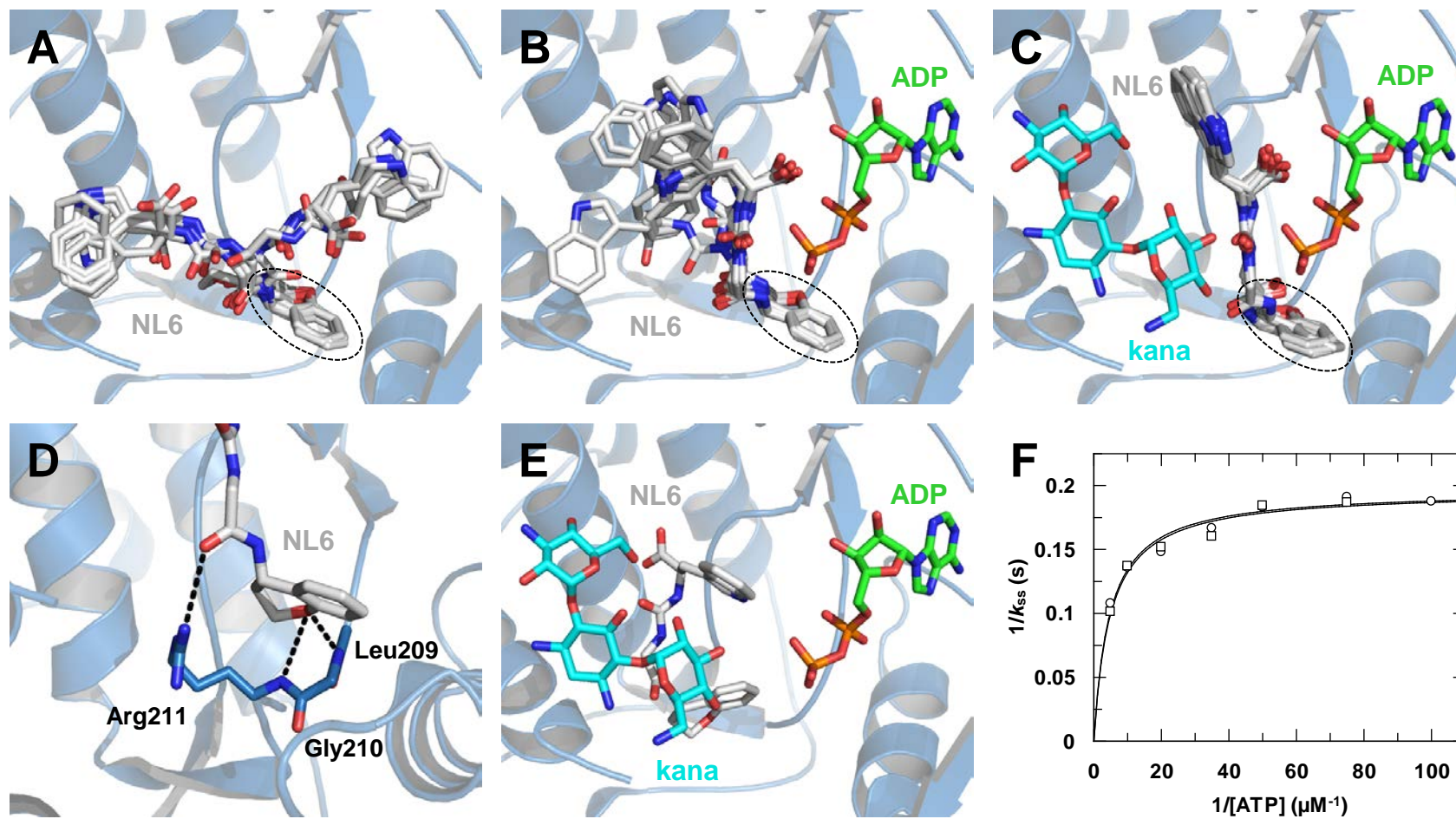


Figure 5

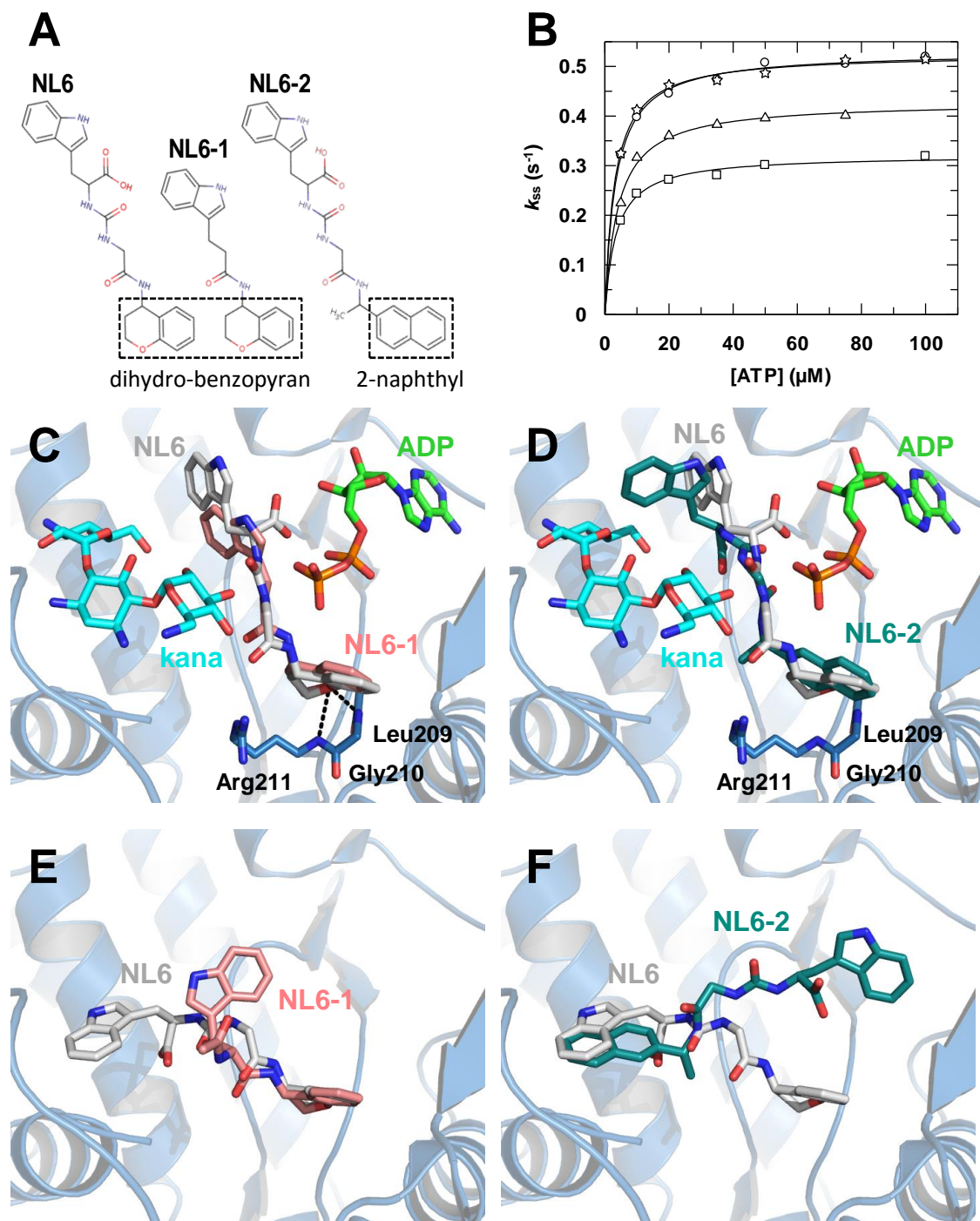
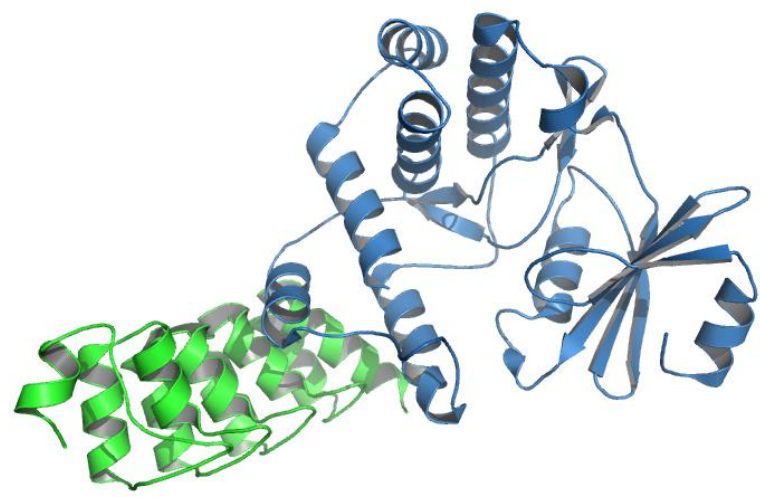


Figure 6

**A**



**B**



**C**



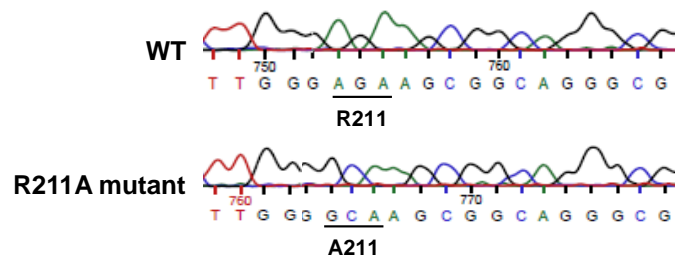


**Fig. S1.** Sequencing result showing the representative part of the *aph(3')-IIIa* gene where the R211A mutation has been introduced.

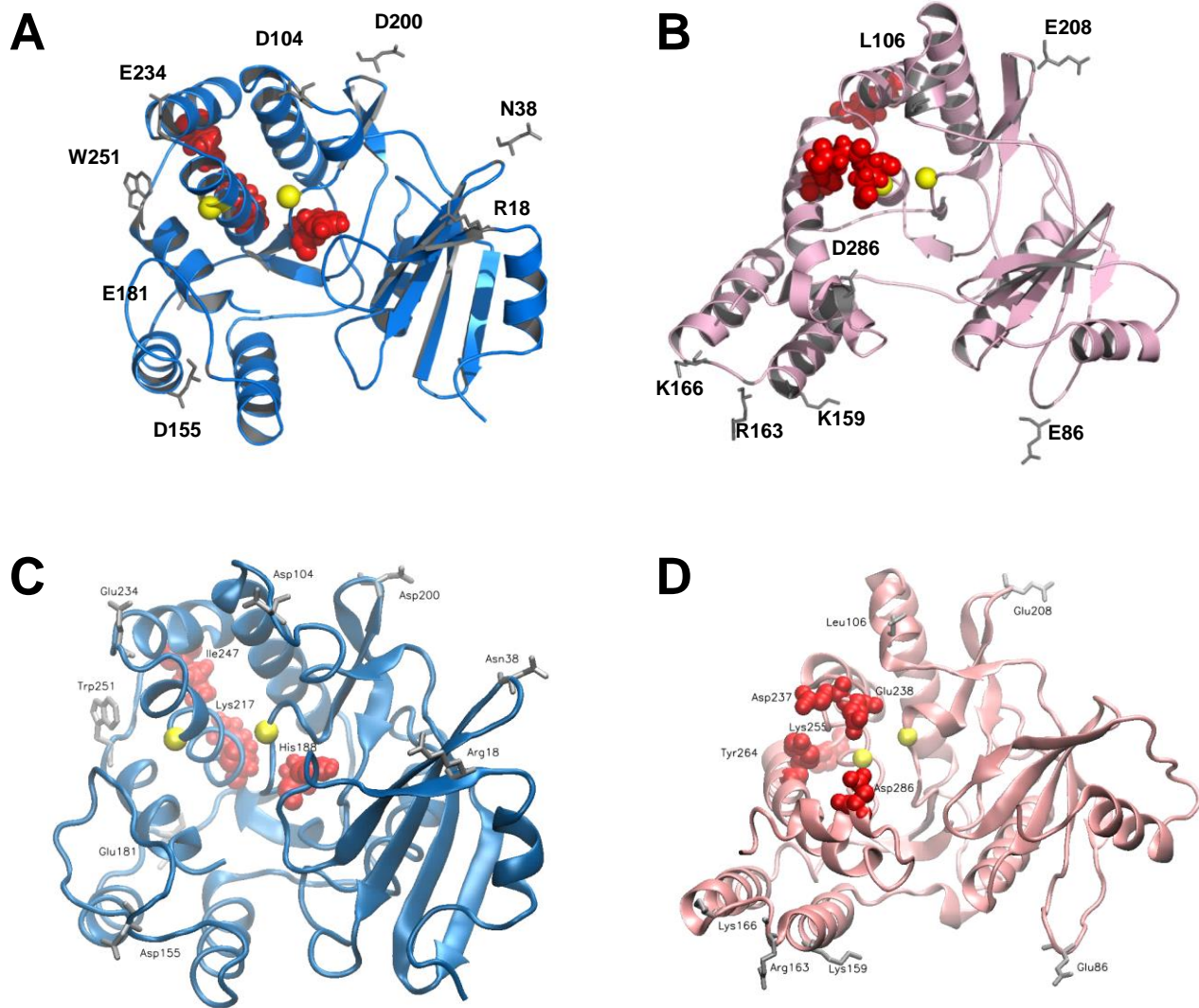


**Fig. S2.** Identification of the target cavities using normal mode analysis. (A, B) Crystal structures of APH(3')-IIIa and APH(2'')-IVa shown as blue or pink cartoon, respectively. The fluctuated residues involved in the cavity are shown as red balls: H188, K217 and I247 in APH(3')-IIIa and D237, E238 and K255 in APH(2'')-IVa. Yellow balls indicate CA atoms of the residues surrounding each cavity (G192 and R226 in APH(3')-IIIa and S199 and S232 in APH(2'')-IVa). (C, D) Movies showing the motions of APH(3')-IIIa and APH(2'')-IVa from superposed normal modes. Same representations as in A and B, respectively.



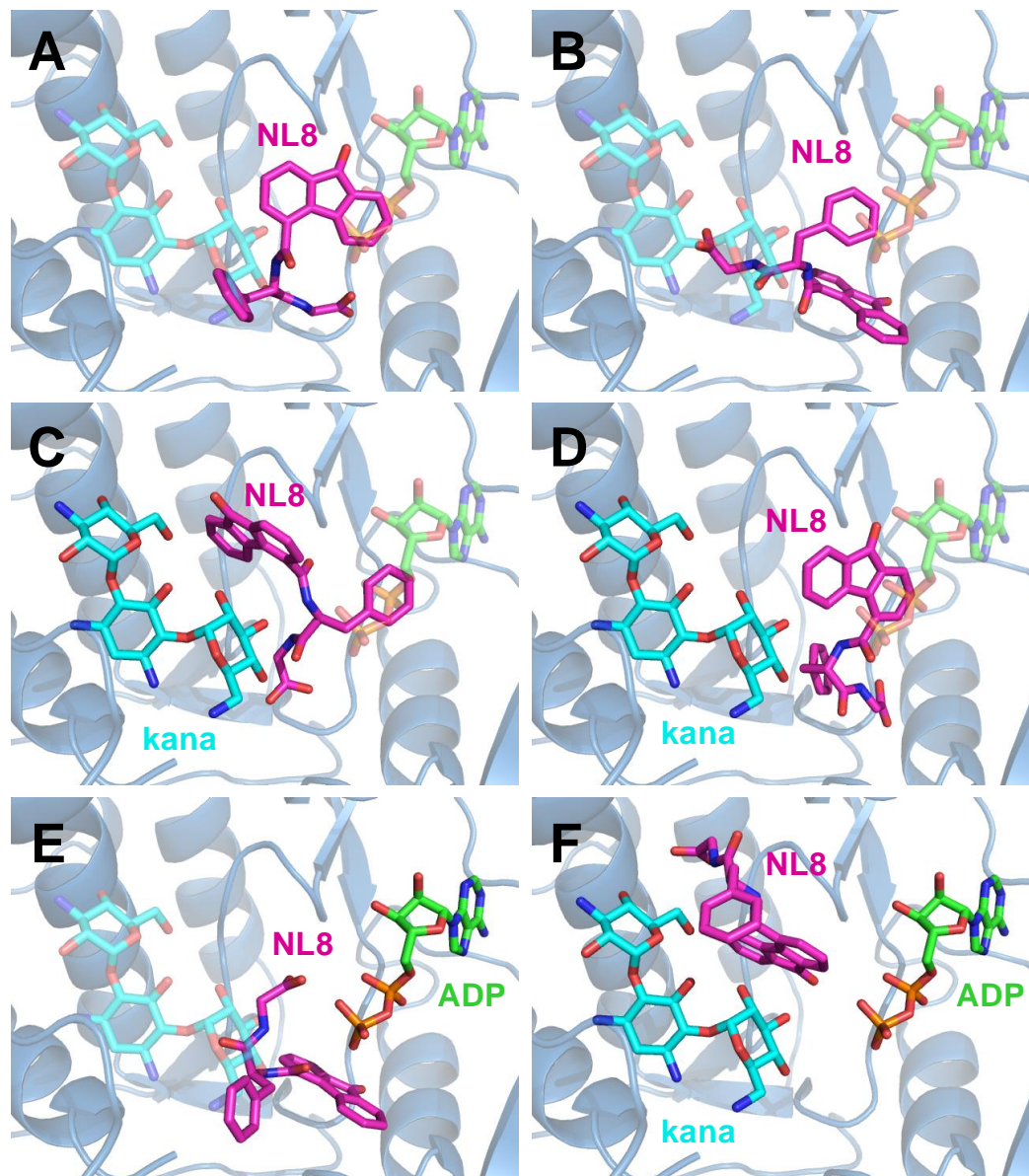


**Fig. S3.** Predicted binding poses obtained for NL8 by molecular docking using identical parameters either in the APH(3')-IIIa apo protein (A, B) or in the APH(3')-IIIa-kanamycin A complex (C, D). Best docking poses of NL8 in the ADP-bound structure (E) or in the ternary complex (F). NL8 was docked into the 1L8T structure in which none, one or both ligands were conserved for docking. Removed ligands are shown in transparent sticks.

**Video Fig S2C**

[Click here to download Supplementary Multimedia File: Fig S2C.mpg](#)

**Video Fig S2D**

[Click here to download Supplementary Multimedia File: Fig S2D.mpg](#)



**Supplementary Multimedia File**

[Click here to download Supplementary Multimedia File: Supplementary material with video.pptx](#)